A Journal of the Gesellschaft Deutscher Chemiker

Angewandte International Edition GDCh Chemie

www.angewandte.org

Accepted Article

Title: Polymorphism of 2D Imine Covalent Organic Frameworks

Authors: Yusen Li, Linshuo Guo, Yongkang Lv, Ziqiang Zhao, Yanhang Ma, Weihua Chen, Guolong Xing, Donglin Jiang, and Long Chen

To be cited as: *Angew. Chem. Int. Ed.* 10.1002/anie.202015130

Link to VoR: https://doi.org/10.1002/anie.202015130

WILEY-VCH

10.1002/anie.202015130

WILEY-VCH

RESEARCH ARTICLE

Polymorphism of 2D Imine Covalent Organic Frameworks

*Yusen Li,[+] Linshuo Guo,[+] Yongkang Lv, Ziqiang Zhao, Yanhang Ma, Weihua Chen, Guolong Xing, Donglin Jiang, and Long Chen**

Abstract: *Isomerism is widely observed in chemistry but it has scarcely been identified in crystalline porous covalent organic frameworks. Herein, we designed and synthesized a series of A_2B_2 type tetraphenyl benzene monomers (p-, m-, and o-TetPB) which have the para-, meta, and ortho-substituted isomeric structures, for the direct construction of isomeric frameworks. Interestingly, both kagome (**kgm**) and monoclinic square (**sql**) framework isomers are produced from either p-TetPB (C_{2h} symmetry) or m-TetPB (C_{2v} symmetry) by simply changing reaction solvents, while their isomeric structures are unambiguously characterized by X-ray diffraction, computational simulation, microscopy, and sorption isotherm measurements. In contrast, only **sql** frameworks was formed for o-TetPB (C_{2v} symmetry), irrespective of reaction solvents. These results disclose a unique feature in the framework structural formation, i.e. the geometry of monomers directs and dominates the lattice growth process while the solvent plays a role in the perturbation of chain growth pattern. The isomeric frameworks exhibit highly selective adsorption of vitamin B_{12} owing to a great difference in their pore shape and size. These results open the possibility of selective crystallization of COFs and topological engineering of the polymorphism of 2D organic materials.*

Introduction

Isomerism is a common phenomenon in chemistry, as it has been developed in small molecules,[1] nanoclusters,[2] porous organic cages (POCs),[3] and metal organic frameworks (MOFs)[4-8]. It has been demonstrated that isomerism is closely correlated to the synthetic conditions including solvents, temperature, nucleation kinetics, and other factors.[1-4] The isomers usually feature significant differences in both structure and function which greatly enhance the structure diversity and application scope. Nevertheless, how to control the isomerism or, in other words, to produce the desired isomer in a selective way remains a challenging goal. This becomes far much difficult in the case of polymer networks, as it requires the same confined growth for all covalent bonds across the material while covalent bond usually lacks precise spatial directivity.

Covalent organic frameworks (COFs) are a class of crystalline porous polymers which have recently drawn even increasing research interest.[9] COFs have been rapidly developed owing to their fascinating designable topologies[10] and broad application prospects in catalysis,[11] photoelectric devices,[12] drug delivery,[13] energy storage,[14] and sensors.[15] The topology of COFs can be well regulated by changing the building blocks, so that various COFs with different topologies have been designed.[10] However, the investigation of the isomerism of COFs remains to be well explored. Examples are limited to only 3D COF-300[16a], 2D COF-ED[16b] and on-surface synthesized single-layered COFs.[16c] The typical 3D COF-300 with a *dia-c5* topology[17] can be converted to an interpenetration isomer with a *dia-c*7 topology when an additional aging process was performed ahead of the conventional synthetic procedure,[16a] and this is based on the interpenetration isomerism.[16a] Co-condensation of D_{2h} symmetric 4′,4‴,4⁗,4⁗′-(ethene-1,1,2,2-tetrayl)tetrakis([1,1′-biphenyl]-4-carbaldehyde]) (ETTBC) and C_2 symmetric 2,5-diaminotoluene (DAT) yields dual-pore kagome or single-pore rhombic frameworks in different solvents.[16b] Theoretically, co-condensation of D_{2h} and C_2 symmetric monomers can generate both kagome and rhombic isomers. However, experimentally most cases yield only one of the isomers.[18]

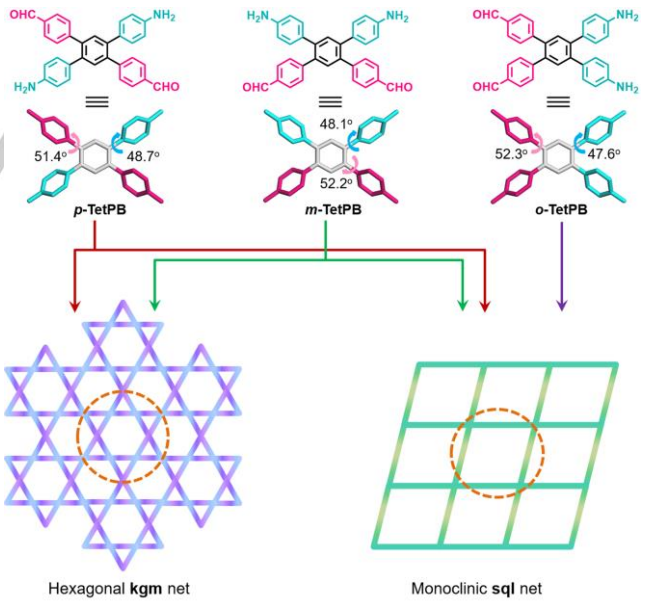

Chart 1. Possible topologies constructed by A_2B_2 monomers of *p*-TetPB, *m*-TetPB, and *o*-TetPB.

Except boroxine-linked COFs[19a] and covalent triazine frameworks (CTFs),[19b] most COFs are constructed by polycondensation of at least two monomers with different reactive groups. Thus, screening specific mixed-solvent systems is a must

[*] Y. Li,[+] Y. Lv, Z. Zhao, G. Xing, Prof. L. Chen
Department of Chemistry, Institute of Molecular Plus and Tianjin Key Laboratory of Molecular Optoelectronic Science, Tianjin University, Tianjin 300072, China.
E-mail: long.chen@tju.edu.cn (L. Chen)
L. Guo,[+] Prof. Y. Ma
School of Physical Science and Technology, Shanghai Tech University, Shanghai 201210, China.
Prof. W. Chen
College of Chemistry and Green Catalysis Center, Zhengzhou University, Henan 450001, China.
Prof. D. Jiang
Department of Chemistry, Faculty of Science, 3 Science Drive, Singapore 117543, Singapore
[+] These authors contributed equally to this work.

Supporting information for this article is given via a link at the end of the document.

10.1002/anie.202015130

for balancing reaction and crystallization to synthesize high quality crystalline COFs.[9,10] Meanwhile, a relative high temperature and long reaction time are generally required to allow the error correction of dynamic covalent linkages.[9e] We recently developed a "two-in-one" molecular design strategy for the high throughput synthesis of COFs *via* self-polycondensation of bifunctional A_2B_2 monomers. A distinct feature is that high quality COFs can be synthesized in various solvents even including low boiling point solvents like dichloromethane (DCM) or methanol.[20] Interestingly, the monomer concentration exerts a minimal influence on the crystallinity of COFs.[20b] Therefore, we envision that the excellent adaptability of this "two-in-one" strategy toward solvents, temperature, and concentration might provide a new possibility for exploring unprecedented isomerism of COFs.

Herein, we elaborately designed and synthesized three A_2B_2 isomeric monomers to construct imine-linked 2D COFs *via* self-polycondensation. These three A_2B_2 monomeric isomers feature same tetraphenyl benzene core (TetPB) but with formyl and amino substituents aligned at different positions (relative to the central benzene ring), named as *p*-TetPB, *m*-TetPB and *o*-TetPB, respectively (Chart 1). DFT calculation revealed that the dihedral angles between the 4-aminophenyl and 4-formylphenyl groups and the central benzene core caused by the steric hindrance between the adjacent phenyl rings were in the range of 47.6°~52.3°, and are nearly identical to each other among the three isomeric TetPB monomers. Regarding the symmetries of *p*-TetPB (C_{2h}) and *m*-TetPB (C_{2v}), both of them are able to assemble into two possible topologies of hexagonal kagome (**kgm**) net and monoclinic square (**sql**) framework (Chart 1, Scheme S4 and S5). These two monomers exhibit similar Gibbs free energy with negligible difference of ΔG = 0.6124 kcal/mol (ESI), suggesting a comparable thermodynamic stability. In contrast, although *o*-TetPB possess the same symmetry with *m*-TetPB (C_{2v}), it can only afford **sql** net due to the configuration mismatch (Chart 1 and Scheme S6). Actually, crystalline TetPB-COFs can be readily synthesized in at least eight different solvents (Figure S1, S5 and S9) to show a good solvent adaptability similar to our previous studies.[20] Moreover, the **kgm** *p*-TetPB-COF-K and *m*-TetPB-COF-K were readily formed in some aprotic solvents such as THF and dioxane while the **sql** *p*-TetPB-COF-M and *m*-TetPB-COF-M were usually obtained in protic alcohols and the optimal solvents for **kgm** and **sql** frameworks were determined to be THF and *n*-BuOH, respectively as judged by the higher surface areas and better PXRD patterns (Figure S1 and S5).

The resulted TetPB-COFs with same chemical constitutions but different topologies are unambiguously characterized and confirmed powder X-ray diffraction (PXRD), high-resolution transmission electron microscope (HRTEM), and pore-size distribution analysis. Theoretically, both *p*-TetPB and *m*-TetPB can yield **kgm** (denote as: TetPB-COF-K, K refers to Kagome) and monoclinic **sql** topologies (denote as: TetPB-COF-M, M stand for monoclinic), while *o*-TetPB only affords a monoclinic **sql** product. We emphasize that it is impossible to obtain framework isomers by the conventional [C_4 + C_4] co-condensation of 1,2,4,5-tetrakis-(4-formylphenyl)benzene (TetPB-4CHO) and 1,2,4,5-tetrakis-(4-aminolphenyl)benzene (TetPB-4NH_2) (Scheme S9). Moreover, the TetPB-COFs with different pore shape and size were employed to adsorb vitamin B_{12} and demonstrated that these isomeric COFs enable selective adsorption and separation. The successful synthesis of COF isomers with different structures and properties from isomeric monomers provide an approach to regulate the polymorph of COFs in a selective manner while enhancing the structural complexity and function scope.

Results and Discussion

Three A_2B_2 monomers (*p*-TetPB, *m*-TetPB and *o*-TetPB) were synthesized via stepwise Suzuki coupling (Scheme S1-S3) and unambiguously characterized by NMR (Figure S34-S48), high resolution ESI mass (Figure S49-S51), and the detailed synthetic procedures were summarized in the Supplementary Information. TetPB-COFs were synthesized as light-yellow powders in high yields (> 85%) from various organic solvents such as dioxane, tetrahydrofuran (THF), *n*-butanol (*n*-BuOH), DCM, *etc.* (Figure S1, S5 and S9). These as-synthesized TetPB-COFs exhibit similar Fourier transform infrared spectra (FT-IR). The characteristic stretching vibration bands for amino and formyl groups were significantly attenuated or even disappeared while the characteristic signals of C=N newly appeared around 1618 cm^{-1} after self-condensation (Figure 1a and S13), indicating these TetPB-COFs feature the same chemical constitution with high polymerization degree. Solid state ^{13}C CP-MAS NMR spectra of these isomeric TetPB-COFs are similar and the characteristic resonance signals around 156 ppm are observed in all TetPB-COFs (Figure 1b and S14), which further confirm the same chemical constitutions and the presence of C=N linkages. Thermogravimetric analysis (TGA) confirmed all TetPB-COFs did not exhibit significant weight loss until 535 °C under N_2 atmosphere (Figure 1c and S15), revealing excellent thermal stabilities. The solid-state diffuse reflectance K–M spectra revealed that these TetPB-COFs showcased nearly identical broad bands around 396 nm (Figure 1d and S16). Therefore, these TetPB-COFs exhibit almost the same thermal stability and electronic absorption features.

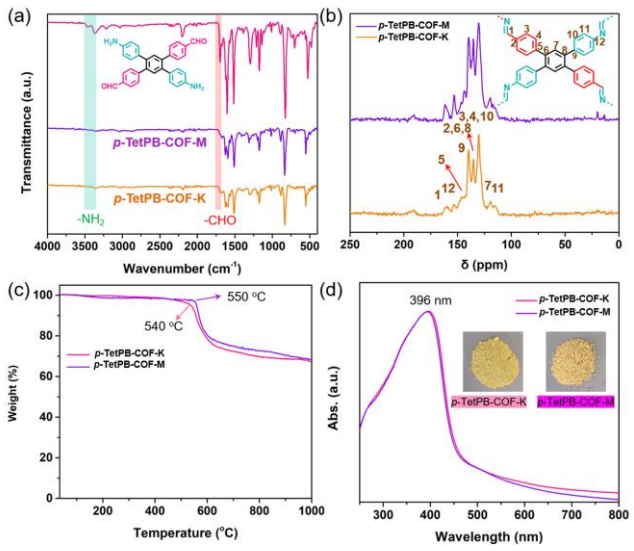

Figure 1. (a) FT-IR spectra comparison of *p*-TetPB-COF-K (orange), *p*-TetPB-COF-M (violet), and *p*-TetPB monomer (pink); (b) Solid-state ^{13}C CP/MAS NMR spectra of *p*-TetPB-COF-K (orange) and *p*-TetPB-COF-M (violet); (c) Thermogravimetric analysis for *p*-TPB-COF-K (pink) and *p*-TetPB-COF-M (violet); (d) UV-visible spectra of *p*-TetPB-COF-K (pink) and *p*-TetPB-COF-M (violet).

10.1002/anie.202015130

WILEY-VCH

RESEARCH ARTICLE

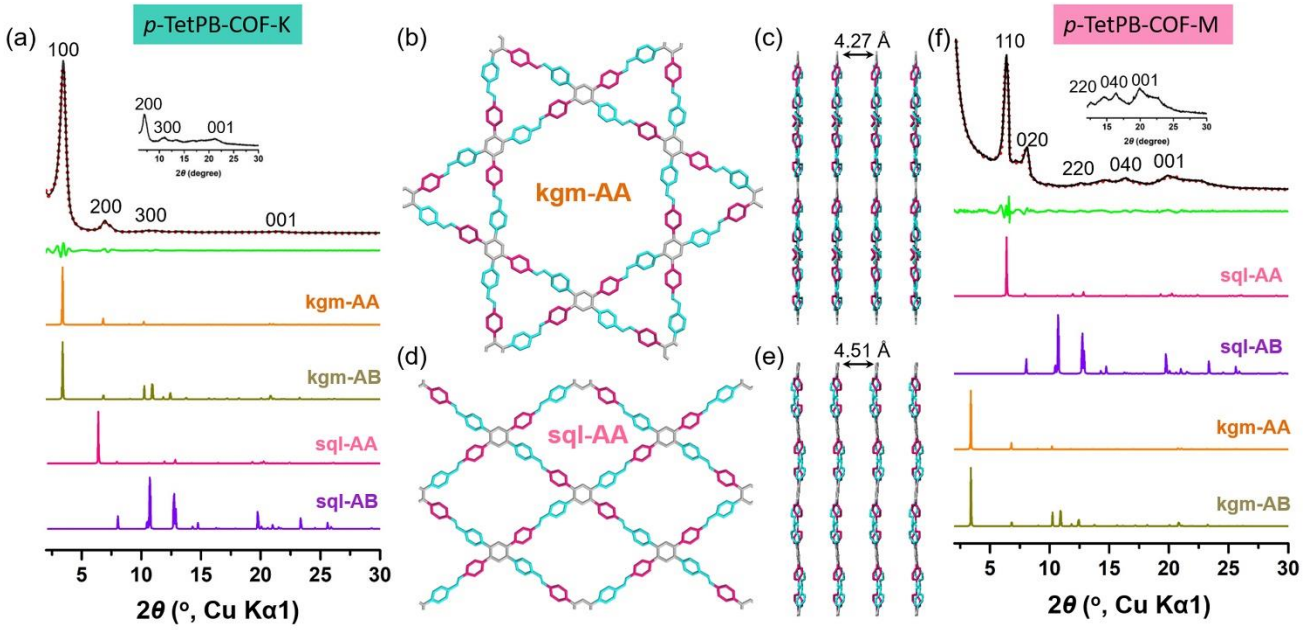

Figure 2. (a) Experimental PXRD patterns of *p*-TetPB-COF-K (black), Pawley refinement (red dot), their difference (green), simulated profiles for kagome **kgm**-AA model (orange), **kgm**-AB model (dark yellow) monoclinic **sql**-AA model (pink) and **sql**-AB model (purple); (b) Top and (c) across views of **kgm**-AA model; (d) Top and (e) across views of **sql**-AA model; (f) Experimental PXRD patterns of *p*-TetPB-COF-M (black), Pawley refinement (red dot), their difference (green), simulated profiles for monoclinic **sql**-AA model (pink), **sql**-AB model (purple), kagome **kgm**-AA model (orange), **kgm**-AB model (dark yellow).

PXRD analysis and structural simulation were performed to assess the crystalline structures of these TetPB-COFs. Taking *p*-TetPB-COFs (Figure 2) as examples to briefly illustrate the structural analysis. The *p*-TetPB-COF-K showcases diffraction peaks at 3.45°, 7.16°, 10.95° and 21.46°, which was consistent well with the simulated eclipsed AA-stacking **kgm** topology and the optimized unit cell parameters are $a = b = 30.04$ Å, $c = 4.27$ Å, $\alpha = \beta = 90°$, and $\gamma = 120°$ (Figure S22 and table S1). The deviations of Pawley refinement were negligible ($R_p = 1.90\%$, $R_{wp} = 2.96\%$) and the diffraction peaks were related to (100), (200), (300), and (001) lattice planes, respectively (Figure 2a, b, c). In contrast, *p*-TetPB-COF-M exhibits diffraction peaks at 6.36°, 8.03°, 12.74°, 16.30°, and 20.06°, which was in accordance with the eclipsed AA-stacking **sql** net. Pawley refinement of the experiment PXRD pattern yielded a unit cell of $a = 17.05$, $b = 24.85$ Å, $c = 4.51$ Å, $\alpha = \gamma = 90°$, and $\beta = 103.36°$ (Figure S23 and Table S2) with good agreement factors ($R_p = 2.84\%$, $R_{wp} = 4.08\%$), and the diffraction peaks were ascribed to (110), (020), (220), (040), and (001) lattice planes (Figure 2d, e, f). Notably, a mixed-phase product could be obtained in propanol which shown both characteristic PXRD signals at 3.45° and 6.36° (Figure S1, dark yellow line).

On the other hand, the kagome and monoclinal *m*-TetPB-COFs exhibited nearly identical PXRD patterns with that of *p*-TetPB-COFs which indicates they possess almost same crystal structures (Figure S24~26, Table S4~S5). The simulated unit cells are $a = b = 30.06$ Å, $c = 4.27$ Å, $\alpha = \gamma = 90°$, $\beta = 120°$ for *m*-TetPB-COF-K and $a = 16.95$ Å, $b = 24.96$ Å, $c = 4.52$ Å, $\alpha = \gamma = 90°$, and $\beta = 103.67°$ for *m*-TetPB-COF-M. The deviations of Pawley refinement with the experimental results were negligible as well ($R_p = 2.06\%$ and $R_{wp} = 3.02\%$ for *m*-TetPB-COF-K, $R_p = 4.26\%$ and $R_{wp} = 5.99\%$ for *m*-TetPB-COF-M). In contrast, exclusive **sql** topological *o*-TetPB-COF was obtained when *o*-TetPB was utilized as the building unit (Scheme S6). The corresponding PXRD pattern exhibited characteristic peaks at 6.42°, 8.02°, 12.95°, 16.36°, and 20.12° (Figure S27) and agreed well with the eclipsed AA-stacking monoclinic model with a unit cell of $a = 16.95$ Å, $b = 24.84$ Å, $c = 4.51$ Å, $\alpha = \gamma = 90°$, and $\beta =$

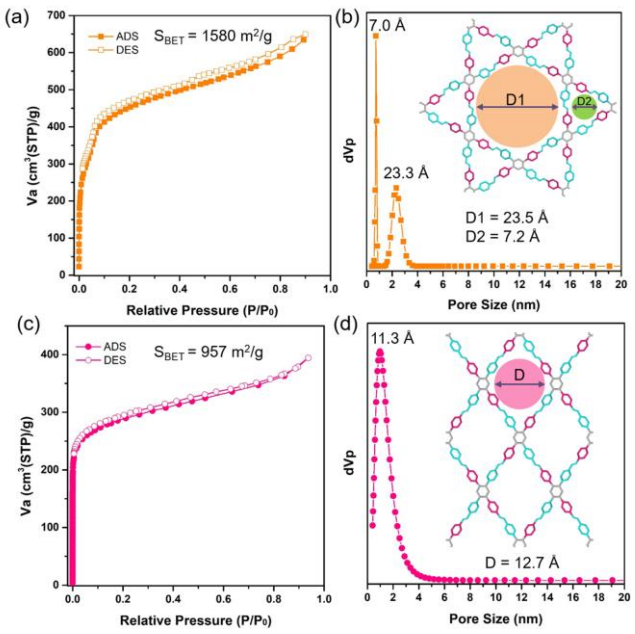

Figure 3. Nitrogen adsorption (solid) and desorption (open) isotherms at 77 K for (a) *p*-TetPB-COF-K synthesized in THF and (c) *p*-TetPB-COF-M synthesized in *n*-BuOH; Pore size distribution curves based on NLDFT calculation for (b) *p*-TetPB-COF-K and (d) *p*-TetPB-COF-M.

10.1002/anie.202015130

WILEY-VCH

RESEARCH ARTICLE

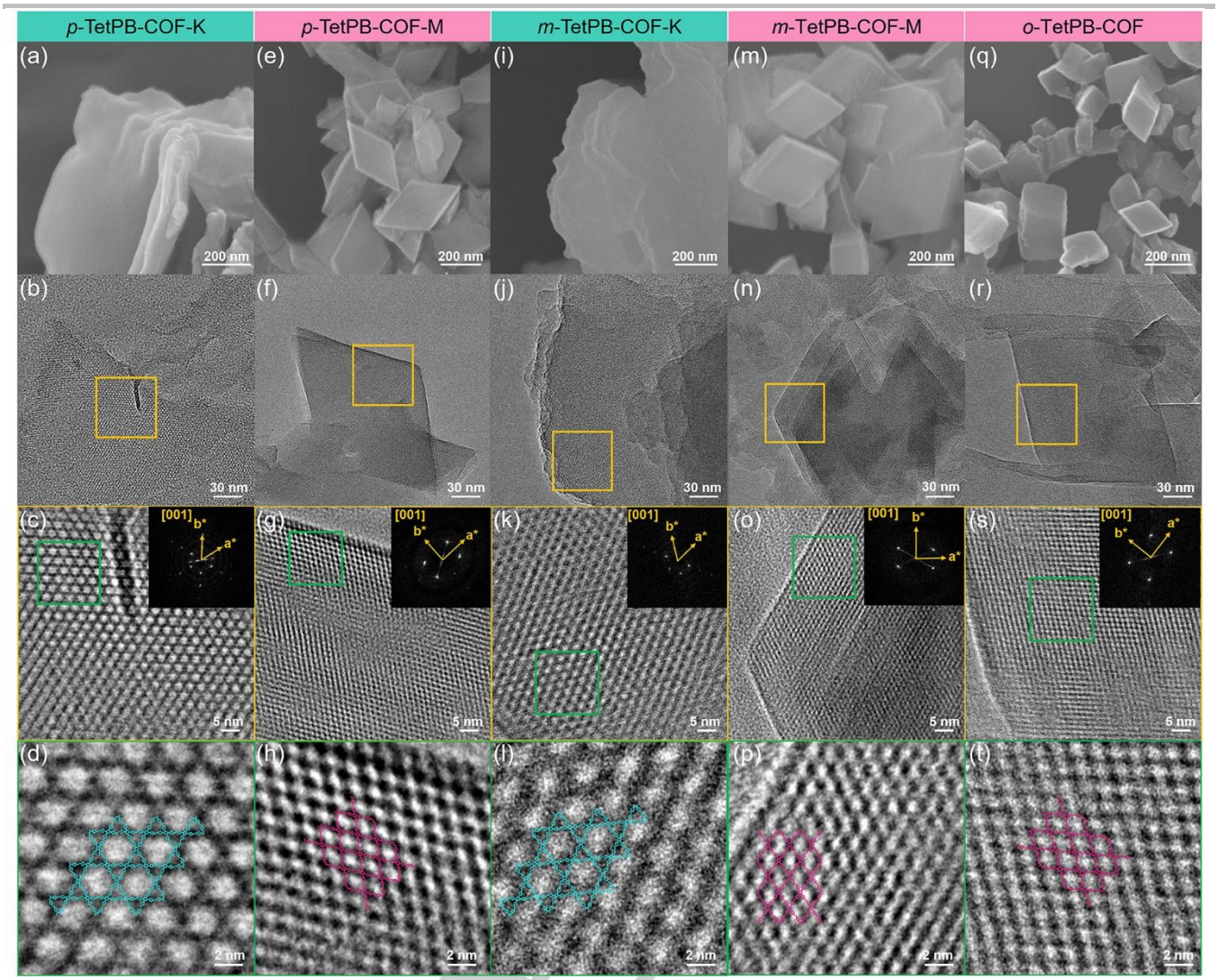

Figure 4. (a) SEM image of *p*-TetPB-COF-K; (b-c) HRTEM images of *p*-TetPB-COF-K, inset pattern is diffractogram obtained from the yellow square area; (d) denoised image of the green square area in image (c) by ABSF filter; (e) SEM image of *p*-TetPB-COF-M; (f-g) HRTEM images of *p*-TetPB-COF-M, inset pattern is diffractogram obtained from the yellow square area; (h) denoised image of the green square area in image (g) by ABSF filter; (i) SEM image of *m*-TetPB-COF-K; (j-k) HRTEM images of *m*-TetPB-COF-K, inset pattern is diffractogram obtained from the yellow square area; (l) denoised image of the green square area in image (k) by ABSF filter; (m) SEM image of *m*-TetPB-COF-M; (n-o) HRTEM images of *m*-TetPB-COF-M, inset pattern is diffractogram obtained from the yellow square area; (p) denoised image of the green square area in image (o) by ABSF filter; (q) SEM image of *o*-TetPB-COF; (r-s) HRTEM images of *o*-TetPB-COF, inset pattern is diffractogram obtained from the yellow square area; (t) denoised image of the green square area in image (s) by ABSF filter.

104.32° (Figure S28 and Table S7). The residuals for Pawley refinement were R_p = 3.95% and R_{wp} = 5.37%, and the diffraction peaks can be reasonably ascribed to the (110), (020), (220), (040), and (001) lattice planes, respectively.

The intrinsic porosity of these isomeric TetPB-COFs was evaluated by nitrogen sorption isotherm measurements at 77 K. As shown in Figure 3a, the isotherms of *p*-TetPB-COF-K exhibited rapid uptake at low pressure (P/P_0 < 0.05) and an obvious step behind P/P_0 = 0.1, which suggesting the coexistence of micropores and mesopores. In sharp contrast, *p*-TetPB-COF-M showcased typical type I sorption isotherms (Figure 3c) indicating the exclusive presence of micropore. The pore volume for *m*-TetPB-COF-K (1.493 cm^3/g calculated at P/P_0 = 0.93, Figure S20a) is greater than that of *p*-TetPB-COF-K (1.158 cm^3/g, Figure 3a), but the isotherms of them are similar. Moreover, the isotherms for *m*-TetPB-COF-M (Figure S20c) and *o*-TetPB-COF (Figure S21a) resemble that of *p*-TetPB-COF-M. Brunauer–Emmett–Teller (BET) surface areas for **kgm** topological *p*-TetPB-COF-K and *m*-TetPB-COF-K are 1580 m^2/g and 1770 m^2/g which are higher than their **sql** topological isomers (957 m^2/g for *p*-TetPB-COF-M, 991 m^2/g for *m*-TetPB-COF-M) and *o*-TetPB-COF (1080 m^2/g). These results are comparable to the theoretical values (ca. 1728 m^2/g for TetPB-COF-K and 1267 m^2/g for TetPB-COF-M) calculated by HT-CADSS approach.[9d] Moreover, the pore size distribution profiles simulated by the nonlocal density functional theory (NLDFT) further clarified the different structures of TetPB-COFs. As shown in Figure 3b, *p*-TetPB-COF-K exhibited a micropore of 7.0 Å and a mesopore of 23.3 Å which agree with the geometrical values (7.2 Å and 23.5 Å). In contrast, *p*-TetPB-COF-M (Figure 3d) only possesses a micropore of 11.3 Å, which is closed to the simulated pore size (12.7 Å). In addition, the pore sizes calculated from the sorption isotherms of *m*-TetPB-

10.1002/anie.202015130

COF-K (7.3 Å and 24.5 Å), *m*-TetPB-COF-M (12.3 Å) and *o*-TetPB-COF (12.1 Å) are all consistent well with the theoretical values (Figure S20b, d and S21b). These results further verified the successful construction of the isomeric **kgm** and **sql** TetPB-COFs.

The morphologies and pore structures of TetPB-COFs were examined by scanning electron microscopy (SEM) and transmission electron microscopy (TEM) (Figure 4, S17, S18 and S19), respectively. Interestingly, the **kgm** topological *p*-TetPB-COF-K (Figure 4a and S17a,b) and *m*-TetPB-COF-K (Figure 4i and S18a,b) exhibited flake-like morphology while **sql** *p*-TetPB-COF-M (Figure 4e and S17c,d), *m*-TetPB-COF-M (Figure 4m and S18c,d), and *o*-TetPB-COF (Figure 4q and S19) assume regular rhombic shape which is rather rare for 2D COFs. The distinct morphologies are probably related to the different reaction solvents.[21] Furthermore, the crystalline structures of these isomeric TetPB-COFs were confirmed by HRTEM. As illustrated in Figure 4, the HRTEM images of *p*-TetPB-COF-K taken along the [001] direction revealed a clear hexagonal honeycomb structure (Figure 4b-c). The denoised image provides clearer bright and dark contrasts which can be attributed to the open channels of the **kgm** network (Figure 4d). On the other hand, the uniform rhombic pore structure can also be clearly visualized in the HRTEM images of *p*-TetPB-COF-M (Figure 4f,g) and the denoised pattern (Figure 4h) shows good bright and dark contrasts. Similarly, the regular kagome and rhombic pore structures of *m*-TetPB-COF-K (Figure 4j-l), *m*-TetPB-COF-M (Figure 4n-p), and *o*-TetPB-COF (Figure 4r-t) also can be directly observed in their corresponding HRTEM images.

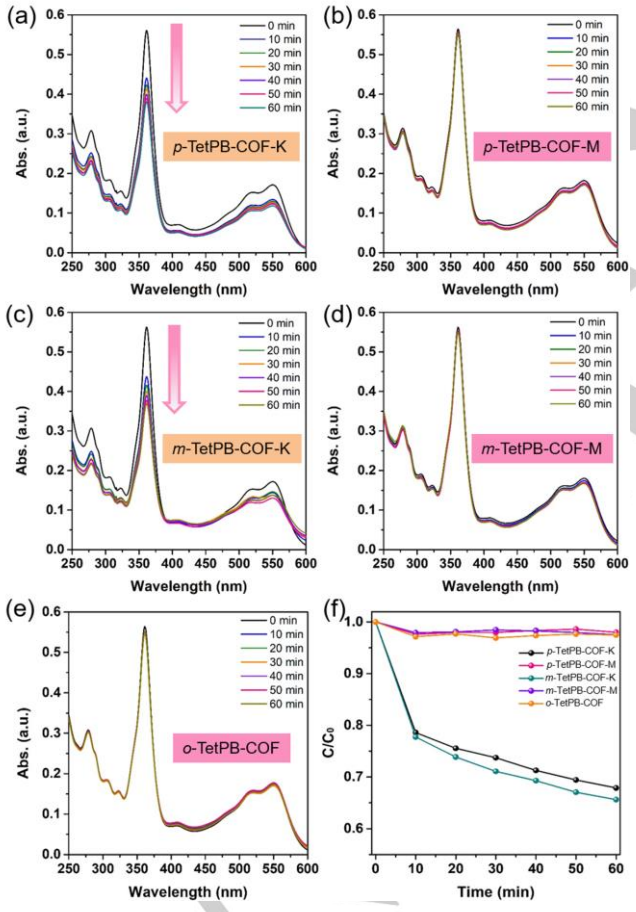

Figure 5. UV−Vis absorption spectra of the aqueous solutions of vitamin B_{12} in the presence of (a) *p*-TetPB-COF-K, (b) *p*-TetPB-COF-M, (c) *m*-TetPB-COF-K, (d) *m*-TetPB-COF-M, and (e) *o*-TetPB-COF at different time intervals. Almost no adsorption in sql TPB-COFs systems after 60 min; (f) Adsorption isotherms of vitamin B_{12} for *p*-TetPB-COF-K (black), *p*-TetPB-COF-M (pink), *m*-TetPB-COF-K (dark cyan), *m*-TetPB-COF-M (violet), and *o*-TetPB-COF (orange).

To provide more insights into the isomerism, the influences of reaction time, temperature and concentration on the crystallization process were systematically investigated. The time dependent PXRD patterns revealed that both TetPB-COF-K and TetPB-COF-M were directly formed without obvious crystal phase transformation processes (Figure S3 and S7). Crystalline *p*-TetPB-COF-K and *m*-TetPB-COF-K were generated at about 1 h (Figure S3a) and 3h (Figure S7a). However, it required at least 9 h to form ordered structure of *p*-TetPB-COF-M (Figure S3b) and *m*-TetPB-COF-M (Figure S7b) which demonstrating the nucleation rate of TetPB-COF-K is faster than that of TetPB-COF-M. On the other hand, as shown in Figure S2a and Figure S6a, crystalline **kgm** *p*-TetPB-COF-K and *m*-TetPB-COF-K were readily synthesized in THF over a wide temperature range (from R.T. to 120 °C). In contrast, highly ordered **sql** *p*- TetPB-COF-M and *m*-TetPB-COF-M could only be obtained at relative high temperature (120 °C) in *n*-BuOH. Oligomers or amorphous polymers were generated when the reaction temperature was below 80 °C (Figure S2b and S6b). This phenomenon may be ascribed to the lower relative total energy of the **kgm** networks than that of the **sql** frameworks (Table S3 and S6). Similarly, the **sql** topological *o*-TetPB-COF also cannot be obtained at relative low temperatures (Figure S10), which indicates the synthetic solvents exert a profound effect on the nucleation process. Moreover, once the synthetic solvent is fixed, the concentration of these isomeric monomers has been demonstrated to exert minimal influence on the topological structures of the corresponding TetPB-COFs (Figure S4, S8 and S12).

To differentiate the characteristic features of these isomeric TetPB-COFs, adsorption experiments of vitamin B_{12} were performed considering the significant difference of the pore size and pore shape of the kagome and monoclinic TetPB-COFs. The molecular dimension of vitamin B_{12} is 14.12 Å×18.35 Å×11.4 Å,[22] which is accessible to the hexagonal mesoporous channels of *p*-TetPB-COF-K and *m*-TetPB-COF-K (~23.5 Å) but should not be compatible to the triangular micropores (~7.2 Å) and inaccessible to these monoclinic frameworks with rhombic micropores (~12.7 Å). The adsorption experiments of vitamin B_{12} were performed by soaking the five different TetPB-COF isomers (15 mg) in an aqueous solution of vitamin B_{12} (30 μg/mL, 50 mL), while the loading amounts of vitamin B_{12} were determined by UV-Vis spectroscopy. As expected, both *p*-TetPB-COF-K and *m*-TetPB-COF-K adsorb vitamin B_{12} because the characteristic absorbance at 361 nm was continued to decline after immersing the **kgm** TetPB-COFs into the solution (Figure 5a, c, f). However, almost no adsorption was observed in the case of **sql** *p*-TetPB-COF-M, *m*-TetPB-COF-M, and *o*-TetPB-COF (Figure 5b-5f). Consequently, the drastic difference in pore characters renders TetPB-COF isomers able to selective adsorb or separate specific guest molecules even though they possess the same chemical composition.

Conclusion

In summary, we have shown the selective growth of isomeric covalent organic lattices to create specific topologies by designing monomer isomers and tuning reaction conditions. Systematic and comparative studies on three monomer isomers with tetraphenyl benzene core and A_2B_2 bifunctionality reveal the production of five different 2D TetPB-COF isomers in a pre-designable yet synthetically controllable manner. Interestingly, TetPB-COFs with different topologies (**kgm** and **sql**), pore shapes and sizes were selectively synthesized from the same A_2B_2 monomers (either *p*-TetPB or *m*-TetPB) by changing reaction solvents. In contrast, **sql** *o*-TetPB-COF was the sole product of *o*-TetPB owing to its restricted configuration. Notably, the long-range ordered kagome and rhombic lattices of these isomeric frameworks are clearly visualized by HRTEM images. With their different pore shape and size, the selective adsorption of vitamin B_{12} become possible, which suggest a great potential of targeted adsorption or separation. This strategy casts a sharp contrast to the conventional co-condensation [C_4 + C_4] approach which cannot form any framework polymorphisms. We highlight that the monomer isomerism is directly transformed into the framework, thus greatly expanding the approaches and scope of the polymorphism of COFs. Considering together with the fact of a broad diversity of monomer isomers, we envision that this approach opens a way to a library of COF polymorphism with different compositions and unprecedented structures.

Acknowledgements

This work was financially supported by the National Key Research and Development Program of China (2017YFA0207500), National Natural Science Foundation of China (51973153, 21975049, 21875140), and the Natural Science Foundation of Tianjin (17JCJQJC44600)

Conflict of interest

The authors declares no conflict of interest.

Keywords: covalent organic frameworks, isomers, controllable growth, selective adsorption.

[1] a) S. Datta, M. L. Saha, P. J. Stang, *Acc. Chem. Res.* **2018**, *51*, 2047-2063; b) O. N. Kavanagh, D. M. Croker, G. M. Walker, M. J. Zaworotko, *Drug. Discov. Today.* **2019**, *24*, 796-804.

[2] a) Z.-J. Guan, F. Hu, J.-J. Li, Z.-R. Wen, Y.-M. Lin, Q.-M. Wang, *J. Am. Chem. Soc.* **2020**, *142*, 2995-3001. b) S. Tian, Y. Z. Li, M. B. Li, J. Yuan, J. Yang, Z. Wu, R. Jin, *Nat. Commun*. **2015**, *6*, 8667.

[3] K. Jie, Y. Zhou, E. Li, F. Huang, *Acc. Chem. Res*. **2018**, *51*, 2064-2072.

[4] T. D. Bennett, A. K. Cheetham, *Acc. Chem. Res*. **2014**, *47*, 1555−1562.

[5] J. Ma, L. D. Tran, A. J. Matzger, *Cryst. Growth Des*. **2016**, *16*, 4148−4153.

[6] J. Pang, S. Yuan, J. Qin, C. Liu, C. Lollar, M. Wu, D. Yuan, H.-C. Zhou, M. Hong, *J. Am. Chem. Soc.* **2017**, *139*, 16939-16945.

[7] F. Igoa, S. Martínez, K. P. S. Zanoni, J. Castiglioni, L. Suescun, J. González-Platas, A. S. S. D. Camargo, C. Kremera, J. Torres, *CrystEngComm*, **2018**, *20*, 4942-4953.

[8] a) B. Karadeniz, D. Žilić, I. Huskić, L. S. Germann, A. M. Fidelli, S. Muratović, I. Lončarić, M. Etter, R. E. Dinnebier, D. Barišić, N. Cindro, T. Islamoglu, O. K. Farha, T. Friščić, K. Užarević, *J. Am. Chem. Soc.* **2019**, *141*, 19214-19220; b) S.-H. Lo, L. Feng, K. Tan, Z. Huang, S. Yuan, K.-Y. Wang, B.-H. Li, W.-L. Day, G. S. Liu, S.; Yang, C.-C. Tao, T.-T. Luo, C.-H. Lin, S.-L. Wang, S. J. L. Billinge, K.-L. Lu, Y. J. Chabal, X. Zou, H.-C. Zhou, *Nat. Chem.*, **2020**, *12*, 90–97.

[9] a) S. Y. Ding, W. Wang, *Chem. Soc. Rev.* **2013**, *42*, 548-568; b) Y. Jin, Y. Hu, W. Zhang, *Nat. Rev. Chem.* **2017**, *1*, 0056; c) Z. Xie, Y. Li, L. Chen, D. Jiang, *Acta Polym. Sin.*, **2016**, *12*, 1621–1634. d) Q. Yang, D. Liu, C. Zhong, J.-R. Li, *Chem. Rev*. **2013**, *113*, 8261−8323. e) J. Á. Martín-Illán, D. Rodríguez-San-Miguel, C. Franco, I. Imaz, D. Maspoch, J. Puigmartí-Luis, F. Zamora, *Chem. Commun.*, **2020**, *56*, 6704–6707.

[10] a) K. Geng, T. He, R. Liu, K. T. Tan, Z. Li, S. Tao, Y. Gong, Q. Jiang, D. Jiang, *Chem. Rev.* **2020**, *120*, 8814–8933. b) N. Huang, L. Zhai, D. E. Coupry, M. A. Addicoat, K. Okushita, K. Nishimura, T. Heine, D. Jiang, *Nat. Commun*. **2016**, *7*, 12325.

[11] a) P. F. Wei, M. Z. Qi, Z. P. Wang, S. Y. Ding, W. Yu, Q. Liu, L. K. Wang, H. Z. Wang, W. K. An, W. Wang, *J. Am. Chem. Soc*. **2018**, *140*, 4623-4631; b) X. Wang, L. Chen, S. Y. Chong, M. A. Little, Y. Wu, W. H. Zhu, R. Clowes, Y. Yan, M. A. Zwijnenburg, R. S. Sprick, A. I. Cooper, *Nat. Chem*. **2018**, *10*, 1180-1189.

[12] a) D. Bessinger, L. Ascherl, F. Auras, T. Bein, *J. Am. Chem. Soc.* **2017**, *139*, 12035-12042; b) H. Ding, J. Li, G. Xie, G. Lin, R. Chen, Z. Peng, C. Yang, B. Wang, J. Sun, C. Wang, *Nat. Commun*. **2018**, *9*, 5234.

[13] a) Q. Fang, J. Wang, S. Gu, R. B. Kaspar, Z. Zhuang, J. Zheng, H. Guo, S. Qiu, Y. Yan, *J. Am. Chem. Soc*. **2015**, *137*, 8352-8355; b) L. Bai, S. Z. F. Phua, W. Q. Lim, A. Jana, Z. Luo, H. P. Tham, L. Zhao, Q. Gao, Y. Zhao, *Chem. Commun*. **2016**, *52*, 4128−4131; c) G. Zhang, X. Li, Q. Liao, Y. Liu, K. Xi, W. Huang, X. Jia, *Nat. Commun*. **2018**, *9*, 2785.

[14] a) S. Wang, Q. Wang, P. Shao, Y. Han, X. Gao, L. Ma, S. Yuan, X. Ma, J. Zhou, X. Feng, B. Wang, *J. Am. Chem. Soc.* **2017**, *139*, 4258-4261; b) X. Chen, Y. Li, L. Wang, Y. Xu, A. Nie, Q. Li, F. Wu, W. Sun, X. Zhang, R. Vajtai, P. M. Ajayan, L. Chen, Y. Wang, *Adv. Mater.* **2019**, *31*, 1901640.

[15] a) X. Liu, D. Huang, C. Lai, G. Zeng, L. Qin, H. Wang, H. Yi, B. Li, S. Liu, M. Zhang, R, Deng, Y. Fu, L. Li, W. Xue, S. Chen, *Chem. Soc. Rev.* **2019**, *48*, 5266−5302; b) Z. Li, N. Huang, K. H. Lee, Y. Feng, S. Tao, Q. Jiang, Y. Nagao, S. Irle, D. Jiang, *J. Am. Chem. Soc.* **2018**, *140*, 12374-12377; c) H. Yuan, N. Li, J. Linghu, J. Dong, Y. Wang, A. Karmakar, J. Yuan, M. Li, P. J. S. Buenconsejo, G. Liu, H. Cai, S. J. Pennycook, N. Singh, D. Zhao, *ACS Sens*. **2020**, *5*, 1474–1481.

[16] a) T. Ma, J. Li, J. Niu, L. Zhang, A. S. Etman, C. Lin, D. Shi, P. Chen, L.-H. Li, X. Du, J. Sun, W. Wang, *J. Am. Chem. Soc*. **2018**, *140*, 6763-6766; b) R.-R. Liang, F.-Z. Cui, R.-H. A, Q.-Y. Qi, X. Zhao, *CCS Chem*. **2020**, *2*, 139–145; c) Y.-P. Mo, X.-H. Liu, D. Wang, *ACS Nano* **2017**, *11*, 11694−11700.

[17] F. J. Uribe-Romo, J. R. Hunt, H. Furukawa, C. Klöck, M. O'Keeffe, O. M. Yaghi, *J. Am. Chem. Soc.* **2009**, *131*, 4570−4571.

[18] a) T.-Y. Zhou, S.-Q. Xu, Q. Wen, Z.-F. Pang, X. Zhao, *J. Am. Chem. Soc*. **2014**, *136*, 15885−15888; b) Z.-F. Pang, T.-Y. Zhou, R.-R. Liang, Q.-Y. Qi, X. Zhao, *Chem. Sci*., **2017**, *8*, 3866–3870; c) F. Auras, L. Ascherl, A. H. Hakimioun, J. T. Margraf, F. C. Hanusch, S. Reuter, D. Bessinger, M. Doblinger, C. Hettstedt, K. Karaghiosoff, *J. Am. Chem. Soc*. **2016**, *138*, 16703−16710.

[19] a) A. P. Côté, A. I. Benin, N. W. Ockwig, M. O'Keeffe, A. J. Matzger, O. M. Yaghi, *Science* **2005**, *310*, 1166−1170; b) P. Kuhn, M. Antonietti, A. Thomas, *Angew. Chem. Int. Ed.* **2008**, *47*, 3450−3453; *Angew. Chem*. **2008**, *120*, 3499–3502

[20] a) Y. Li, W. Chen, G. Xing, D. Jiang, L. Chen, *Chem. Soc. Rev*., **2020**, *49*, 2852-2868; b) Y. Li, Q. Chen, T.; Xu, Z. Xie, J. Liu, X. Yu, S. Ma, T. Qin, L. Chen, *J. Am. Chem. Soc.* **2019**, *141*, 13822−13828; c) W. Hao, D. Chen, Y. Li, Z. Yang, G. Xing, J. Li, L. Chen, *Chem. Mater.* **2019**, *31*, 8100−8105; d) X. Yan, H. Liu, Y. Li, W. Chen, T. Zhang, Z. Zhao, G. Xing, L. Chen, *Macromolecules* **2019**, *52*, 7977−7983; e) D. Chen, W. Chen, G. Xing, T. Zhang, L. Chen, *Chem. Eur. J.* **2020**, *26*, 8377–8381; f) B. Zhang, X. Song, Y. Li, Y. Li, Z. Peng, L. Ye, L. Chen, 2 *Chem. Commun* **2020**, *56*, 3253-3256.

[21] G. Das, T. Skorjanc, S. K. Sharma, F. Gándara, M. Lusi, D. S. S. Rao, S. Vimala, S. K. Prasad, J. Raya, D. S. Han, R. Jagannathan, J.-C. Olsen, A. Trabolsi, *J. Am. Chem. Soc.* **2017**, *139*, 9558−9565.

[22] D. C. Hodgkin, J. Kamper, M. Mackay, J. Pickworth, K. N. Trueblood, J. G. White, *Nature* **1956**, *178*, 64–66.

10.1002/anie.202015130

WILEY-VCH

Layout 2:

RESEARCH ARTICLE

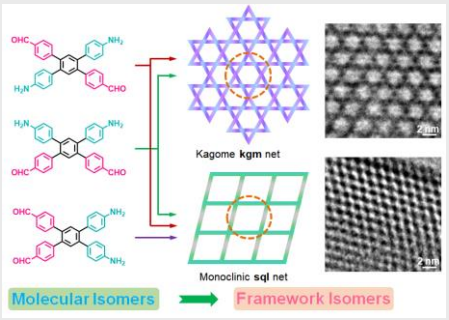

*Y. Li,⁺ L. Guo,⁺ Y. Lv, Z. Zhao, Y. Ma, W. Chen, G. Xing, D. Jiang, L. Chen**

Page No. – Page No.

Polymorphism of 2D Imine Covalent Organic Frameworks

An efficient strategy was developed for selective growth of isomeric covalent organic frameworks by designing monomer isomers and tuning reaction conditions. Three elaborately designed A_2B_2 type tetraphenyl benzene monomers (*p*-, *m*-, and *o*-TetPB) successfully afford the corresponding five different 2D TetPB-COF isomers in a pre-designable yet synthetically controllable manner, which exhibit selective adsorption of vitamin B_{12} owing to a great difference in their pore shape and size.